Application of Karhunen-Loève Expansions for the Dynamic Analysis of a Natural Convection Loop for Known Heat Flux

Tobias Hummel[a], **Arturo Pacheco-Vega**[b1]

[a]Department of Mechanical Engineering, Technische Universität München, Boltzmannstraße 15 85748 Garching, Germany
[b]Department of Mechanical Engineering, California State University, Los Angeles, Los Angeles, CA 90032, USA

E-mail: apacheco@calstatela.edu

Abstract. In the present study we use Karhunen-Loève (KL) expansions to model the dynamic behavior of a single-phase natural convection loop. The loop is filled with an incompressible fluid that exchanges heat through the walls of its toroidal shape. Influx and efflux of energy take place at different parts of the loop. The focus here is a sinusoidal variation of the heat flux exchanged with the environment for three different scenarios; i.e., stable, limit cycles and chaos. For the analysis, one-dimensional models, in which the tilt angle and the amplitude of the heat flux are used as parameters, were first developed under suitable assumptions and then solved numerically to generate the data from which the KL-based models could be constructed. The method of snapshots, along with a Galerkin projection, was then used to find the basis functions and corresponding constants of each expansion, thus producing the optimal representation of the system. Results from this study indicate that the dimension of the KL-based dynamical system depends on the linear stability of the steady states; the number of basis functions necessary to describe the system increases with increased complexity of the system operation. When compared to typical dynamical systems based on Fourier expansions the KL-based models are, in general, more compact and equally accurate in the dynamic description of the natural convection loop.

1. Introduction

Natural convection loops are important devices used in several engineering applications, among which geothermal energy, solar collectors, energy storage, computer and nuclear reactor cooling, are representative examples [1, 2]. In these thermal systems, the fluid is subjected to heat extraction in certain regions and heat addition in others. The accompanied density gradients generate buoyancy forces, which initiate and sustain a naturally driven flow, transporting thermal energy by convection without the need of external pumping devices. Understanding these systems' time-dependent behavior is important for performance prediction and control. Therefore, toroidal and rectangular loops have been studied both experimentally [3]–[5], and numerically [6]–[8]. From the numerical perspective, both two- and three-dimensional time-dependent models have been developed [9, 10]; however, one-dimensional versions have been

[1] Corresponding author, Tel.: (323) 343-4492, e-mail: apacheco@calstatela.edu

particularly useful to understand the occurrence of chaos in these systems.

The usual approach to the analysis of natural convection loops, since first proposed by Malkus [11], has been the use of Fourier series expansions to transform the governing partial differential equations (PDEs) into a system of ordinary differential equations (ODEs). Though this methodology grants analytical treatment of the governing equations, depending on the type of boundary conditions, the set of ODEs might not always be decoupled [8]. The resulting infinite number of equations complicates their dynamic analysis and hence their control. It may be, therefore, advantageous to apply alternative techniques that may provide accurate models through a finite set of equations.

Karhunen-Loève (KL) decomposition [12, 13], known under different names in other fields [14], is a linear technique that systematically constructs compact models from either experimental or numerical data. The general idea is to extract orthogonal basis functions from an ensemble of given data that contain all the information of the system. These basis functions, with their corresponding constants, represent the characteristics of the system from which the collection was obtained in a mathematically-optimal manner. The technique has been used extensively to build low-order models in turbulence [15], thermal process design [16], and system identification and control [17, 18], among other areas. Preliminary application of the method to the toroidal loop with known wall-temperature condition has been recently reported by Pacheco-Vega and Villarreal-Fonz [19].

In this work we expand the application of the KL technique by developing accurate and compact dynamical models of a thermal convection loop for the case of a known heat flux boundary condition. To this end, the thermal loop is described first. The non-dimensional version of the governing equations, which have previously been studied via Fourier expansions [8], are then provided. A general description of the KL methodology is presented next, followed by numerical solutions of the foregoing equations that will serve as the basis for the development of the dynamical models. Finally, the KL approach, along with a Galerkin projection, is used to build the low-order representations of the thermal loop. The results show that the models developed this way are accurate and, once built, require little CPU time to generate the dynamic performance of the system.

2. Problem Description

The natural circulation loop considered here is depicted in Fig. 1. The loop has a toroidal shape with radius R, built out of tubing of diameter d, filled with an incompressible fluid. The torus can be tilted by an angle α with respect to the horizontal plane, as illustrated in the figure, with one part of it being heated while the other is being cooled. A dotted line serves as reference for the inclination angle and divides the heating ($\pi \leq \theta < 2\pi$) and cooling ($0 \leq \theta < \pi$) regions; θ is the angular coordinate. In a gravitational field, temperature differences within the fluid generate buoyancy forces that set the fluid in motion, transferring heat by convection from the heated section to the cooled one.

In this study, the modeling approach is based on one-dimensional versions of the momentum and energy equations that have been extensively used in the past [6]–[8]. In these, both the fluid velocity u^*, and the temperature T^*, are averaged over the cross-section, so that $u^* = u^*(t^*)$ and $T^* = T^*(t^*, \theta)$, with t^* being time. The symbol $(^*)$ indicates dimensional quantities. By using the Boussinesq approximation for the buoyancy term, and neglecting axial conduction within the fluid, the integral of the momentum equation over the loop and the energy equation are

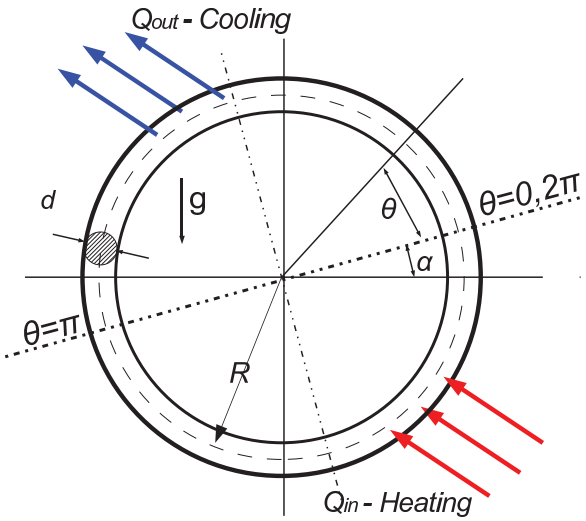

Figure 1. Schematic of a toroidal thermal loop.

given [8] as

$$\frac{du^*}{dt^*} + \frac{4k_f}{\rho_0 d}\, u^* = \frac{\beta g}{2\pi}\int_0^{2\pi} T^* \cos(\theta+\alpha)d\theta, \tag{1}$$

$$\frac{\partial T^*}{\partial t^*} + \frac{u^*}{R}\frac{\partial T^*}{\partial \theta} = \frac{4q^*}{\pi d^2 \rho_0 c_p}, \tag{2}$$

where ρ_0, β, and c_p are the fluid density, thermal expansion coefficient, and specific heat, respectively; g is the gravity constant, k_f is the proportionality constant in the assumed linear relationship between shear stress and mean velocity, and q^* is the externally prescribed heat rate per unit length of the loop. The above equations can be solved for u^* and T^* after q^* is established. Different conditions for q^* may be used [8]. For the present work, we focus on a known heat flux given by $q^* = -\widehat{q}\sin\theta$, where $\widehat{q}$ is the heat amplitude.

Normalization of the Eqs. (1) and (2) can be done by defining

$$u = \frac{4k_f R}{\rho_0 d}u^*; \quad t = \frac{\rho_0 d}{4k_f}t^*; \quad T = \frac{\rho_0^2 d^2 \beta g}{32 k_f^2 R}(T^* - T_0^*); \quad Q_D = \frac{\rho_0^2 d\beta g}{32\pi c_p k_f^3 R}q^*, \tag{3}$$

where T_0^* is a reference temperature. The resulting non-dimensional version of the governing equations are

$$\frac{du}{dt} + u = \frac{1}{\pi}\int_0^{2\pi} T\cos(\theta+\alpha)d\theta, \tag{4}$$

$$\frac{\partial T}{\partial t} + u\frac{\partial T}{\partial \theta} = Q_D, \tag{5}$$

where

$$Q_D = -Q\sin\theta, \quad \text{with} \quad Q = \frac{\rho_0^2 d\beta g}{32\pi c_p k_f^3 R}\widehat{q}. \tag{6}$$

In Eq. (6), Q is a non-dimensional heat flux. It is to be noted that Pacheco-Vega et al. [8] have studied the thermal loop for the known heat flux, and other conditions, using Fourier series expansions.

3. Karhunen-Loève Expansion Technique

Mathematical details of the technique can be found in the literature, e.g., [14, 15, 17, 18]. Thus, only a brief discussion is provided next. Given a set of data, either from experiments or numerical simulations, being represented by functions $\mathcal{U}(x) = \{v_k(x)\}_{k=1}^{\mathcal{K}}$, in a specific domain D_Ω, the main idea of the KL method is to generate an "optimum" set of orthonormal basis functions $\Phi = \{\phi_m\}$ for $m = 1, ..., \mathcal{M}$, for the space spanned by the given set. For each element of $\mathcal{U}$, this is given as

$$v_k(x) = \sum_{m=1}^{\mathcal{M}} a_{km}\phi_m(x), \quad k = 1, ..., \mathcal{K}, \tag{7}$$

where $\mathcal{K}$ is the number of observations, $\mathcal{M}$ the number of terms in the expansion, and x is usually a set of spatial variables. Further it is assumed that $\mathcal{U}$ belongs to a linear infinite-dimensional Hilbert space $\mathcal{L}^2([0,1])$, with the inner product $(\cdot,\cdot)$ and the norm $||\cdot||$.

Based on the procedure outlined by [17, 18], the first step in the KL methodology is to obtain a new set of functions $w_k = v_k - \overline{\mathcal{U}}$ for $k = 1, 2, ..., \mathcal{K}$, locally referenced to the average of the sequence $\overline{\mathcal{U}} = \langle \mathcal{U} \rangle = \frac{1}{\mathcal{K}} \sum_{k=1}^{\mathcal{K}} v_k(x)$. Using this set, we then seek functions ϕ_m that maximize $\langle (w_k, \phi_m)^2 \rangle$ under the restriction $(\phi_m, \phi_m) = ||\phi_m||^2 = 1$. This optimization problem leads to the following eigenvalue problem [15]

$$\mathcal{R}\,\phi_m = \lambda_m \phi_m, \qquad m = 1, ..., \mathcal{M}, \tag{8}$$

where $\mathcal{R}$ is the two-point spatial correlation function (covariance matrix in the discrete case) defined as

$$\mathcal{R}(x, x') = \left\langle w_k(x) w_k(x') \right\rangle. \tag{9}$$

In Eq. (8), $\phi_m(x)$ correspond to the eigenfunctions (or eigenvectors), also known as *KL modes* or *empirical eigenfunctions*, of Eq. (9), and λ_m are the eigenvalues, which are all real and positive. It is important to note that the m-th eigenvalue represents the average energy (captured information) of the m-th eigenfunction.

Two equivalent methodologies, the so-called *direct method* proposed by Lumley [20] in the context of turbulence, and the method of *snapshots* of Sirovich [21] can be used to determine the empirical eigenfunctions ϕ_m of Eq. (7). Because of its efficiency in handling large number of data, here we have used the latter technique.

In the method of *snapshots*, the eigenfunctions can be written as the linear combination

$$\phi_m = \sum_{k=1}^{\mathcal{K}} b_k^m w_k(x), \quad m = 1, \cdots, \mathcal{M}, \tag{10}$$

where $w_k(x)$ is the averaged ensemble of data, and the coefficients b_k^m are such that the set $\Phi = \{\phi_m\}_{m=1}^{\mathcal{M}}$, will resemble the set $\mathcal{V} = \{w_k(x)\}_{k=1}^{\mathcal{K}}$. When w_k is defined at $\mathcal{N}$ spatial points x_n, for $n = 1, ..., \mathcal{N}$, then $w_k(x_n) \equiv \mathbf{v}_k$, and the eigenvalue problem defined in Eq. (8), can be written in vector-matrix form as

$$\mathbf{C}\mathbf{V}^m = \lambda_m \mathbf{V}^m, \tag{11}$$

where the elements of the covariance matrix $\mathbf{C}$, of size $\mathcal{K} \times \mathcal{K}$, are given by

$$C_{kl} = \frac{1}{\mathcal{K}} \int_{D_\Omega} w_k(x') w_l(x') dx', \tag{12}$$

$$= \mathbf{v}_k^T \mathbf{v}_l, \tag{13}$$

for $k, l = 1, \cdots, \mathcal{K}$, and $\mathbf{V}^m = [b_1^m, b_2^m, \cdots, b_{\mathcal{K}}^m]^T$ is the m-th eigenvector. It is important to state that $\mathbf{v} \not\equiv \mathbf{V}$. A decreasing arrangement of the eigenvalues $\lambda_1 > \lambda_2 > ... > \lambda_m > ... > \lambda_{\mathcal{K}}$

indicates a direct relationship between magnitude of the eigenvalue and information carried by the respective eigenvalue. Hence, the interest is on the first $\mathcal{M}$ eigenvalues based on the following energy criterion

$$\frac{\sum_{m=1}^{\mathcal{M}} \lambda_m}{\sum_{k=1}^{\mathcal{K}} \lambda_k} > p, \tag{14}$$

where the value of p is specified by the user based on the desired accuracy of the reconstruction. Once the eigenfunctions ϕ_m in Eq. (7) are determined, the corresponding coefficients, a_{km}, can be found using the well-known Galerkin method of weighted residuals [22].

4. Numerical Solution and Snapshots

The numerical data that will be used to generate the KL basis functions of the dynamical models, come from the solution of Eqs. (4) and (5), along with the boundary condition (6), via the method of finite differences under specific values of the parameters. However, the steady-state versions of the equations are solved analytically before the dynamical solution is numerically determined. The corresponding steady state solutions for u and T are

$$\overline{u} = \pm\sqrt{Q\cos\alpha}; \qquad \overline{T} = \pm\sqrt{\frac{Q}{\cos\alpha}}\,\cos\theta, \tag{15}$$

where the $\pm$ sign in $\overline{u}$ indicates the two possible directions of the flow: counterclockwise $(+)$ or clockwise $(-)$.

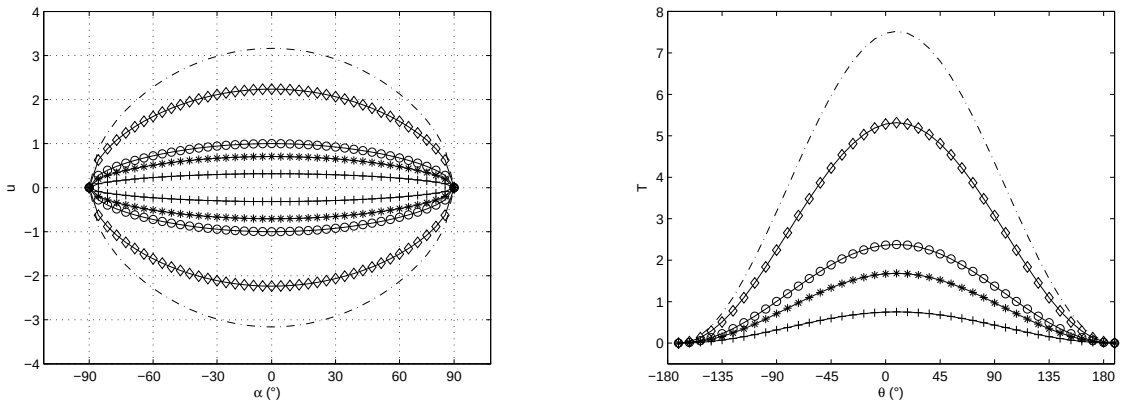

(a) $\overline{u}$ vs. α. (b) $\overline{T}(\theta)$ for $\alpha = 45°$.

Figure 2. Steady-state velocity and temperature profiles for different values of Q. $(-+-)$ 0.1; $(-*-)$ 0.5; $(-\circ-)$ 1; $(-\diamondsuit-)$ 5; $(-\cdot-)$ 10.

The steady-state velocities, found analytically, are shown in Fig. 2(a) as functions of α and Q. In agreement with Pacheco-Vega *et al.* [8], we have found that these exist if the tilt position of the loop is $-90° \leq \alpha \leq 90°$, where a distinct magnitude of each direction occurring for a specific tilt position of the loop. The maximum velocity occurs at zero tilt whereas the minimum (theoretically zero) is at $\alpha = 90°$. Intuitively expected, the foregoing behavior holds true for all magnitudes of prescribed heat rates, with increased magnitudes caused at higher Q-values. On the other hand, the steady-state value of the fluid temperature depends on its location on the loop, as shown in Fig. 2(b) for $\alpha = 45°$. The maximum and minimum values of $\overline{T}$ occur, respectively, at $\theta = 0°$ (where the flow leaves the heating and enters the cooling region) and

at $\theta = 180^\circ$ (where the flow leaves the cooling and enters the heating region). The larger the magnitude of the heat rate, the larger the temperature difference between minimum and maximum values. The value of the tilt angle α has also an enhancing effect for both $\overline{u}$ and $\overline{T}$. The larger tilt angle, the larger temperature differences in the fluid. It is important to point out that the case of a clockwise flow direction, the temperature distribution behaves exactly in an opposite fashion, where the maximum and minimum temperatures occur at the opposite location on the natural convection loop, because the of the reverse flow.

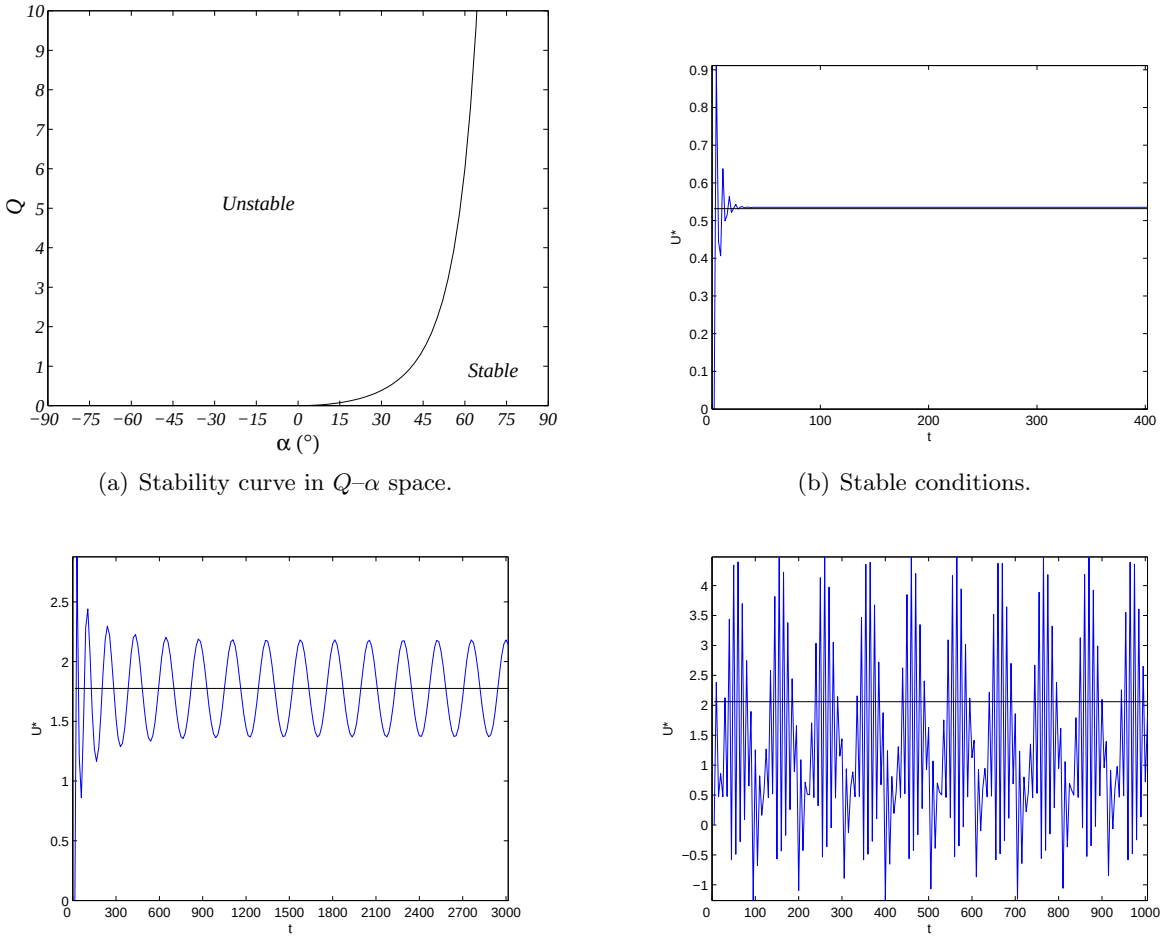

(a) Stability curve in Q–α space.

(b) Stable conditions.

(c) Limit cycles.

(d) Chaotic conditions.

Figure 3. Stability curve and numerical solutions for $u(t)$.

In order to determine the time dependent solutions of the governing PDEs we use an explicit finite differences scheme to integrate the temporal direction, whereas backward differences are chosen for the space discretization. The discretized form of Eqs. (4)–(6) is given by

$$u_i^{k+1} = \frac{1}{1+\Delta t}\left(u_i^k + \frac{\Delta t}{\pi}\sum_{j=1}^{N} T_j^k \cos(\theta_j + \alpha)\Delta\theta\right), \tag{16}$$

$$T_i^{k+1} = T_i^k + \frac{\Delta t}{\Delta\theta}\, u_i^{k+1}(T_{i-1}^k - T_i^k) - \frac{Q\Delta t}{\pi}\sin\theta_i. \tag{17}$$

The foregoing equations are coupled through the velocity term u_i^{k+1}, where the indices $i = 1, 2, ..., N$ and $k = 1, 2, ..., M$ indicate the spatial and temporal direction, respectively. The solution steps to this set has been outlined in Hummel [23]; the coding was implemented in MATLAB. The solutions have been obtained for several values of the parameters Q and α. A typical grid-size of $\pi/300$ was used in the space dimension, whereas the time integration was carried out from $t = 0$ to steady-state, with time increments of $\Delta t = 0.001$ s.

The ensemble of numerical solutions $T(t, \theta)$ (also called snapshots), were determined for different combinations of (α, Q). As noted by c.f. [8], the behavior of the thermal loop changes its character based on α and Q; i.e. for certain values these parameters, the system will be linearly stable or unstable. A linear stability analysis of Eqs. (4) and (5) provides these regions in the parameter space as illustrated in Fig. 3(a). Also shown in the figure is the neutral stability curve. As observed, for certain combinations of (α, Q) the loop is stable, whereas for others it is unstable, giving rise to either a sink, limit cycles or chaos.

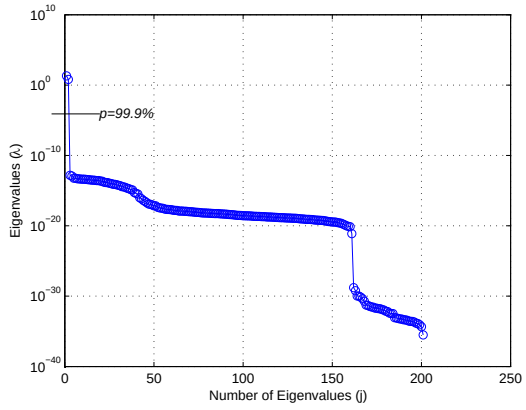

Figure 4. KL modes $\alpha = 45°$; $Q = 0.4$.

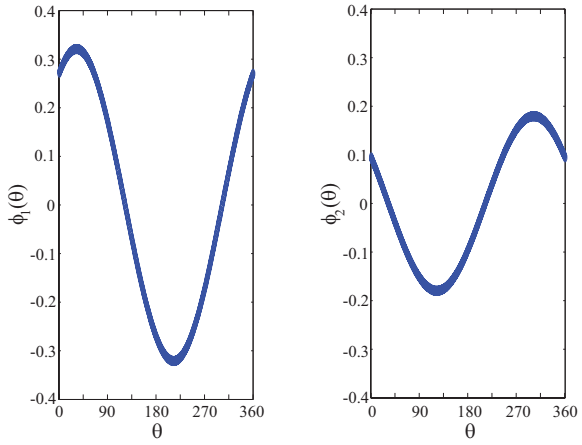

Figure 5. ϕ_1, ϕ_2 for $\alpha = 45°$; $Q = 0.4$.

5. Model Reduction

Once the snapshots are built we apply the KL expansion to construct the dynamical models. To this end, a criterion for p is set as 99% of the possible information about the system, i.e., the energy, captured by the empirical eigenfunctions.

5.1. Stable Conditions

For $\alpha = 45°$ and $Q = 0.4$ the flow is stable. For this condition, Fig. 4 shows the distribution of the KL modes obtained from the eigenvalue problem given by Eq. (11). As observed, for this case the first two eigenvalues have captured 99% of the information; hence requiring only the corresponding first two empirical eigenfunctions ϕ_1 and ϕ_2 to accurately characterize the dynamical behavior of the loop. As expected the basis functions are sinusoidal in shape as shown in Fig. 5. The subsequent basis functions ϕ_3, $\phi_4 ... \phi_{\mathcal{K}}$ quickly loose their distinct sinusoidal character and approach a constant zero value, revealing that they do not carry any significant information.

After the Galerkin projection has been applied to find the constants a_{km} in Eq. (7) qualitative comparison between the numerical solutions, given as surfaces $T(t, \theta)$, and the KL approximations is shown in Fig. 6. Quantitatively, the percentage error between the solutions shown in Figs. 6(a) and 6(c) is actually less than 10^{-10}. The CPU time required to compute the

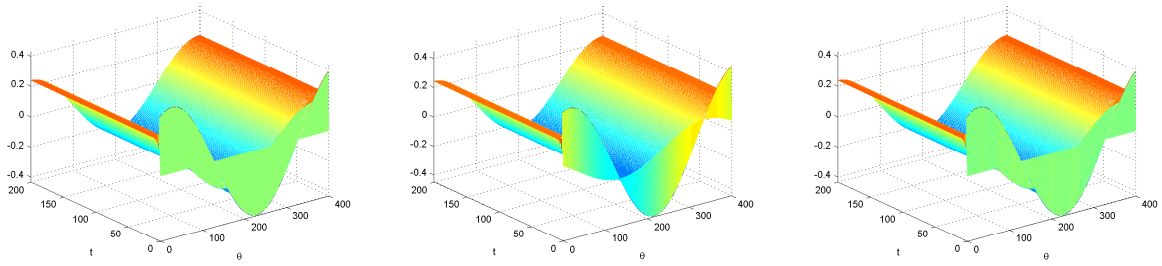

(a) Numerical solution. (b) $\mathcal{M} = 1$. (c) $\mathcal{M} = 2$.

Figure 6. Numerical vs. KL solutions. $\alpha = 45°$; $Q = 0.4$.

solutions with the KL expansion model, using MATLAB as the computer language, is of only one second, and the finite difference integrations take more than five minutes.

5.2. Limit Cycles

For $\alpha = 60°$ and $Q = 6.3$, which reflects the performance of the loop in the region near the neutral stability curve in Fig. 3(a), the dynamic condition give rise to limit cycles. This dynamic condition is characterized as a combination of stable and chaotic dynamics, where the system converges to an evenly oscillating, repetitive pattern around the steady state. The velocity pattern is shown in Fig. 3(c). Similar to the stable case, only the first two eigenvalues provide 99% of the system's information when expanded through the corresponding eigenfunctions, leaving the remaining eigenfunctions needless.

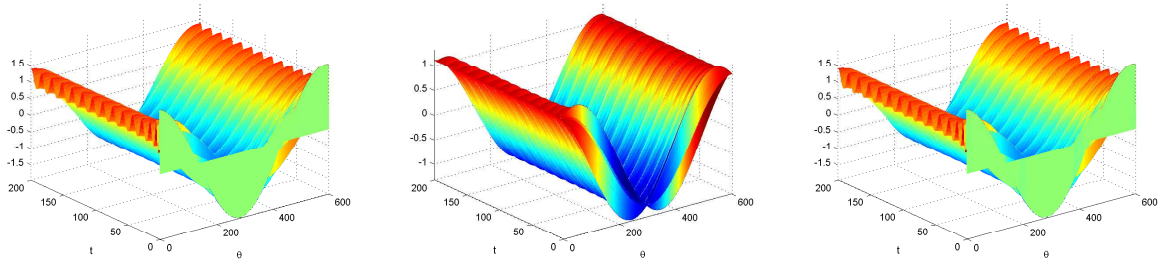

(a) Numerical solution. (b) $\mathcal{M} = 1$. (c) $\mathcal{M} = 2$.

Figure 7. Numerical vs. KL solutions. $\alpha = 60°$; $Q = 6.3$.

For qualitative comparison, Fig. 7 provides the temperature surfaces $T(t, \theta)$ of the numerical solution and the KL reconstructions. The powerful nature of the technique is shown by the percentage error between the numerical and the KL solutions shown in Figs. 7(a) and 7(c), which is less than 10^{-10}, as well as by the CPU time required to compute the solutions being at only two seconds, whereas the finite difference calculations last more than ten minutes.

5.3. Chaos

For $\alpha = 45°$ and $Q = 6.3$, which is an operation point relatively far above the neutral stability curve of Fig. 3(a), the loop achieves chaotic behavior. A characteristic of this dynamic condition, shown in Fig. 3(d), is a complex, unorganized, and strongly fluctuating behavior of the fluid velocity and temperature distribution, without any convergence or repetitive pattern be recognizable. The complex nature of these dynamics requires 33 eigenvalues to provide 99%

of capturing energy. Hence, 33 empirical eigenfunctions are needed in the expansion (7) to transmit all required information for an accurate reconstruction of the dynamic model via KL expansions.

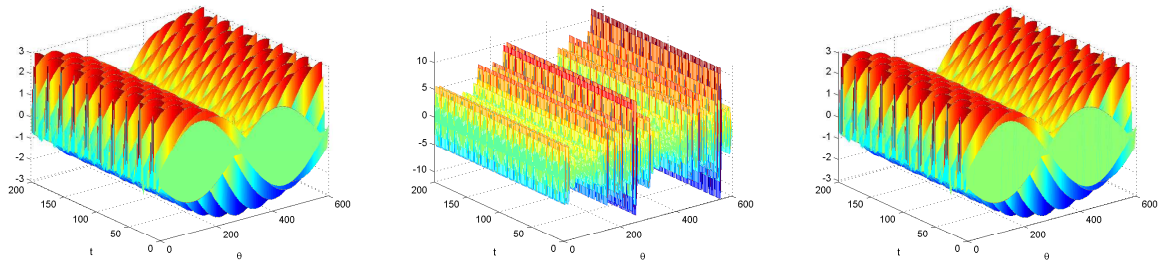

(a) Numerical solution. (b) $\mathcal{M} = 1$. (c) $\mathcal{M} = 33$.

Figure 8. Numerical vs. KL solutions. $\alpha = 45°$; $Q = 6.3$.

The temperature surfaces of a natural convection loop in chaos dynamical conditions are shown in Fig. 8. The numerical- and KL-solutions (with 99% capturing energy), which are shown in Figs. 8(a) and 8(c), are quasi identical –as expected. Fig. 8(b) gives an interesting insight on the effects if only a subset of the significant information; i.e., less than $\mathcal{M} = 33$ eigenfunctions were used for the KL expansions. The resulting dynamical model is then incomplete, and does not represent the behavior of the original system. The percentage error between the numerical and the KL solutions is less than 10^{-5}. The CPU time required to compute the full KL solutions is at one second, whereas the finite difference integrations require more than twelve minutes.

Although not explicitly illustrated here for purposes of compactness, comparison between the KL-expansion-based models and the dynamical system obtained by Pacheco-Vega et al. [8] via Fourier expansions, are shown to be equally accurate. Using the definition of p in Eq. (14), for the stable and limit-cycle conditions the number of eigenfunctions in the two expansion models needed to capture at least 99% of the system information is two. For the case of chaotic conditions, the KL expansion model requires 33 eigenfunctions whereas 40 are needed by the Fourier-based model.

6. Concluding Remarks

Natural convection loops are important in numerous practical applications, where omission of external pumping devices to sustain a fluid flow to transfer thermal energy may be necessary. In this work we have used Karhunen-Loève (KL) expansions to develop low-order dynamic models of these systems. The main advantage offered by the KL technique is that the models constructed are 'optimal' in the least squares sense; so that, for a given level of accuracy, no better model can be found.

Results for different parameter values, for three stability conditions, have shown that the convection loop models built this way provide excellent accuracy with respect to the numerical solutions from which they were derived, but require of only a few seconds of CPU time. For a given level of accuracy, the number of eigenfunctions required to capture the dynamic behavior of the loop increases with its complexity; stable versus chaotic conditions, e.g. only two empirical eigenfunctions were required for stable conditions of the loop whereas 33 basis functions were to be used in chaotic conditions. When compared to typical dynamical systems based on Fourier expansions the KL-based models are, in general, more compact and equally accurate in the dynamic description of the natural convection loop.

Acknowledgments
The authors wish to acknowledge the contribution of K. Villarreal-Fonz towards the development of this work. This work has been partially supported by NSF grants IIP-0724505, IIP-0844891 and HRD-0932421.

7. References

[1] Japikse D 1973 *Advances in Heat Transfer* **9** 1–111
[2] Greif R 1988 *ASME J. Heat Transfer* **110** 1243–1258
[3] Creveling H, DePaz J, Baladi J and Schoenhals R 1975 *J. Fluid Mech.* **67** 65–84
[4] Damerell P S and Schoenhals R J 1979 *ASME J. Heat Transfer* **101** 672–676
[5] Acosta R, Sen M and Ramos E 1987 *Wärme- und Stoffübertragung* **21** 269–275
[6] Greif R, Zvirin Y and Mertol A 1979 *ASME J. Heat Transfer* **101** 684–688
[7] Sen M, Ramos E and Treviño C 1985 *Int. J. Heat Mass Transfer* **28** 219–233
[8] Pacheco-Vega A, Franco W, Chang H C and Sen M 2002 *Int. J. Heat Mass Transfer* **45** 1379–1391
[9] Lavine A G, Greif R and Humphrey J A C 1986 *Int. J. Heat Mass Transfer* **108** 796–805
[10] Desrayaud G, Fichera A and Marcoux M 2006 *International Journal of Heat and Fluid Flow* **27** 154–166
[11] Malkus W 1972 *Mémoires Société Royale des Science de Liége, 6e Série, Vol. IV* 125–128
[12] Karhunen K 1946 *Prozessa Ann. Acad. Sci. Fennicae* **37** 808–817
[13] Loève M 1955 *Probability Theory* (Princeton, N.J.: VanNostrand)
[14] Berkooz G, Holmes P and Lumley L 1993 *Annual Review of Fluid Mechanics* **25** 375–539
[15] Holmes P, Lumley J L and Berkooz G 1996 *Turbulence, Coherent Structures, Dynamical Systems and Symmetry* (USA: Cambridge University Press)
[16] Balsa-Canto E, Alonso A and Banga J 2004 *Journal of Ind. Eng. Chem.* **43** 3353–3363
[17] Ly H V and Tran H T 2001 *Mathematical and Computer Modelling* **33** 223–236
[18] Atwell J and King B 2001 *Mathematical and Computer Modelling* **33** 1–19
[19] Pacheco-Vega A and Villarreal-Fonz K 2008 *Proceedings of the 5th. European Thermal-Sciences Conference* (Eindhoven, The Netherlands) paper No. NCV 16
[20] Lumley J L 1967 *Atmospheric Turbulence and Wave Propagation* ed Yaglom A M and Tatarski V (Nauka, Moscow) pp 166–178
[21] Sirovich L 1987 *Quarterly of Applied Mathematics* **45** 561–571
[22] Wylie C and Barrett L 1995 *Advanced Engineering Mathematics.* (New York, USA: McGraw-Hill Inc.)
[23] Hummel T 2011 *Development of Low-Dimensional models of a Natural Convection Loop with Karhunen-Loève Expansions for Known Heat Flux* (Los Angeles, CA: BS. Thesis, California State University–Los Angeles)